Monthly Notices
of the
ROYAL ASTRONOMICAL SOCIETY

MNRAS **485,** 5590–5597 (2019)
Advance Access publication 2019 March 27

doi:10.1093/mnras/stz841

Precessing winds from the nucleus of the prototype Red Geyser?

Rogemar A. Riffel [1,2]★ Rodrigo S. Nemmen,[3] Gabriele S. Ilha [1,2] Sandro B. Rembold,[1,2] Namrata Roy [4] Thaisa Storchi-Bergmann,[2,5] Rogerio Riffel [2,5] Kevin A. Bundy,[6] Alice D. Machado,[1,2] Nicolas D. Mallman,[2,5] Jaderson S. Schimoia,[1,2,7] Luiz N. da Costa[2,8] and Marcio A. G. Maia[2,8]

[1]*Departamento de Física, Universidade Federal de Santa Maria, CCNE, Santa Maria, RS 97105-900, Brazil*
[2]*Laboratório Interinstitucional de e-Astronomia - LIneA, Rua General José Cristino 77, Rio de Janeiro, RJ 20921-400, Brazil*
[3]*Departamento de Astronomia, Universidade de São Paulo, IAG, São Paulo, SP 05508-090, Brazil*
[4]*Department of Astronomy and Astrophysics, University of California, 1156 High Street, Santa Cruz, CA 95064, USA*
[5]*Universidade Federal do Rio Grande do Sul, IF, CP 15051, Porto Alegre 91501-970, RS, Brazil*
[6]*UCO/Lick Observatory, University of California, Santa Cruz, 1156 High St., Santa Cruz, CA 95064, USA*
[7]*Physics Department, Universidade Federal de Santa Catarina, Florianópolis, SC 88036-000, Brazil*
[8]*Observatório Nacional - MCT, Rua General José Cristino 77, Rio de Janeiro, RJ 20921-400, Brazil*

Accepted 2019 March 19. Received 2019 March 19; in original form 2018 November 11

ABSTRACT

Supermassive black holes (SMBHs) are present at the centre of most galaxies, with the related mass accretion processes giving origin to outflows in active galactic nuclei (AGNs). It has been presumed that only intense winds from luminous AGNs were able to suppress star formation until the discovery of a new class of galaxies with no recent star formation and with the nucleus in a quiescent state showing kpc scale outflows. We used SDSS MaNGA and Gemini Integral Field Spectroscopy of the prototype Red Geyser Akira and found that the orientation of the outflow changes by about 50° from its nucleus to kpc scales. A possible interpretation is that the outflow is produced by a precessing accretion disc due to a misalignment between the orientation of the disc and the spin of the SMBH. The precession of the central source is also supported by a similar change in the orientation of the ionization pattern. Although similar behaviour has commonly being reported for collimated relativistic jets, the precession of an AGN wide wind is reported here for the first time, implying on a larger work surface of the wind, which in turn increases the star formation suppression efficiency of the outflow.

Key words: galaxies: active – galaxies: ISM – galaxies: nuclei – galaxies: star formation.

1 INTRODUCTION

Most galaxies containing a spheroidal component (elliptical galaxies and bulges of spiral galaxies) seem to host a central supermassive black hole (SMBH; Heckman & Best 2014, for a review) that interacts with its host galaxy via capture of matter and emission of radiation, particles and winds from its surroundings. These processes are witnessed in active galactic nuclei (AGNs), and seem to play an important role in the evolution of the host galaxies. Cosmological simulations that do not consider the presence of SMBHs and their mechanisms of feeding and feedback that are present in the AGN phase, result in galaxies that are much more massive than those observed (Benson et al. 2003; Di Matteo, Springel & Hernquist 2005; Springel, Di Matteo & Hernquist 2005; Bower et al. 2006). Massive outflows triggered as a consequence of the accretion process to the SMBH can regulate and couple the growth of the galactic bulge and the SMBH (e.g. Hopkins et al. 2005; Cattaneo et al. 2009), explaining the relation between the mass of the SMBH and stellar velocity dispersion of the bulge. The narrow-line regions (NLRs) are the signposts of the central activity of SMBHs, since they are generally expected to present a bi-symmetric emission pattern in ionized gas (e.g. Antonucci 1993; Urry & Padovani 1995; Harrison et al. 2018). Puzzling enough, *Hubble Space Telescope* (*HST*) narrow-band [O III]λ5007 images of a sample of 60 nearby Seyfert galaxies show that the bi-conical shape of the NLR is not as common as expected (Schmitt et al. 2003) and gas outflows are seen only in 33 per cent of Seyfert galaxies, as revealed by long-slit spectroscopy of 48 nearby AGNs (Fischer et al. 2013). On the other hand, ionized gas outflows in the inner kpc have been commonly observed using optical (e.g. Schnorr-Müller et al. 2014; Cresci et al. 2015; Lena et al. 2015; Karouzos, Woo & Bae 2016a,b; Venturi et al. 2018) and near-infrared (e.g. Barbosa et al. 2014; Riffel, Storchi-Bergmann & Rifffel 2014; Riffel, Hekatelyne & Freitas

★ E-mail: rogemar@ufsm.br

2018) integral field spectroscopy (IFS) of nearby active galaxies. Another puzzling result is that outflows seem to be almost absent for low-luminosity AGNs, showing increasing extent and power as the AGN luminosity increases (e.g. Ilha et al. 2018).

Recently, an intriguing result was reported on a sample of galaxies with no recent star formation activity, most of them harbouring a very low luminosity AGN (LLAGN): a bi-polar outflow seen in ionized gas and interpreted as being originated by centrally driven winds due to a radiatively inefficient accretion flow (RIAF; Yuan et al. 2015) on to the SMBH (Cheung et al. 2016). This study is based on large-scale (several kpc) data cubes obtained by the Sloan Digital Sky Survey 4th phase (SDSS-IV) Mapping Nearby Galaxies at Apache Point Observatory (MaNGA) survey and suggests that such galaxies – dubbed 'Red Geysers' – are very common, accounting for 5–10 per cent of the population of galaxies with stellar masses of $M_\star \sim 5 \times 10^{10}\,\mathrm{M}_\odot$ that do not show recent star formation episodes (Cheung et al. 2016; Roy et al. 2018). These large-scale outflows are capable of suppressing the star formation in this population of galaxies. Penny et al. (2018) reported the detection of analogous galaxies to Red Geysers in low-mass galaxies ($M_\star \leq 5 \times 10^9\,\mathrm{M}_\odot$). However, the angular resolution of the observations (∼3 arcsec) does not allow to constrain the kinematics in the nuclear region and therefore the mechanism that produces the outflows in these galaxies is poorly known.

In order to better constrain the gas kinematics, probing scales three times smaller than those probed by MaNGA, we obtained IFS with Gemini GMOS of the inner 1.7 kpc × 2.5 kpc of *mangaid* 1-217022 – dubbed as Akira – to complement the information from MaNGA IFU data. Akira is the prototype of the Red Geyser class, harbours an LLAGN and presents a well-defined large-scale bipolar outflow (Cheung et al. 2016). It has a redshift $z = 0.0245$, for which 1 arcsec corresponds to ∼500 pc at the distance of the galaxy, adopting a Hubble constant of $H_0 = 71\,\mathrm{km\,s^{-1}\,Mpc^{-1}}$.

In this paper, we report that for Akira the orientation of outflow changes with the distance from the nucleus, with a possible cause being possibly due to the precession of the accretion disc which creates a precessing wind. This paper is organized as follows: Section 2 describes the data used in this work, while in Section 3 we present our results, which are discussed in Section 4. Finally, Section 5 presents the final remarks.

2 DATA AND MEASUREMENTS

2.1 MaNGA data

The MaNGA (Bundy et al. 2015) fibre-bundle IFU survey is part of the SDSS-IV (Gunn et al. 2006; Blanton et al. 2017), uses the Baryon Oscillation Spectroscopic Survey (BOSS; Smee et al. 2013) spectrograph, covering the spectral range from 3622 to 10 354 Å at a resolving power $R \sim 2000$ and will obtain IFU observations of ∼10 000 nearby galaxies spanning all environments and the stellar mass range 10^{9}–$^{11}\,\mathrm{M}_\odot$ at a spatial resolution of 1–2 kpc (Bundy et al. 2015; Drory et al. 2015; Law et al. 2015; Yean et al. 2016b; Wake et al. 2017). The data cube for Akira is included in the 14th Data Release (DR14; Albareti et al. 2017) of the SDSS.

The data processing was performed using the MaNGA Data Reduction Pipeline (Law et al. 2016) and the relative flux calibration of the final spectra is better than 5 per cent (Yan et al. 2016a). Akira was observed with a fibre-bundle of 61 fibres with a diameter of 9 fibres, resulting in a bundle diameter of 22.″5 and the reconstructed FWHM is ∼2.″7.

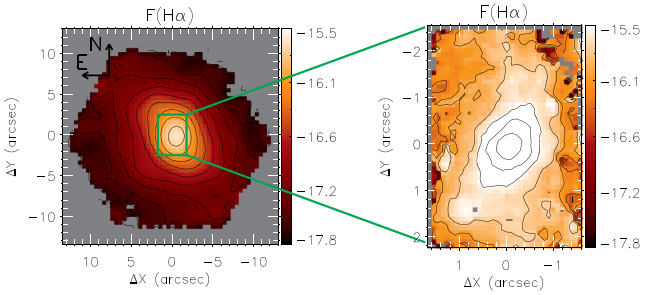

Figure 1. H α emission-line flux map using MaNGA (left) and GMOS (right) data. The colour bars show the fluxes in logarithmic units of erg s^{-1} cm^{-2} arcsec^2.

2.2 Gemini GMOS data

Akira was observed with Gemini Multi-Object Spectrograph (GMOS; Hook et al. 2004) IFU (Smith et al. 2002) on 2017 December 25 (Project: GN-2017B-Q-26). The observations were done in the single-slit mode using the B600 grating, covering the wavelength range from 4350 to 7050 Å and resulting in a Field of View (FoV) of 3.5 arcsec × 5.0 arcsec. Four 1 120 s on-source exposures were done, resulting in a total exposure time of 1.25 h.

We used the IRAF software to perform the data reduction following Lena (2014). The data cubes for each exposure were created at an angular sampling of 0.″1 × 0.″1 and then median combined using the peak of the continuum as reference for astrometry and a sigma-clipping algorithm for bad pixel/cosmic ray removal. The average Differential Image Motion Monitor (DIMM) seeing during the observations was 0.″9.

2.3 Emission-line fitting

We followed the procedure described in Ilha et al. (2018), using the Gas AND Absorption Line Fitting (GANDALF) code (Sarzi et al. 2006; Oh et al. 2011) to fit the emission-line profiles and the underlying stellar continuum for the MaNGA data cube, allowing us to measure simultaneously the gas and stellar kinematics. The underlying stellar contribution on the galaxy spectra is fitted by GANDALF using the Penalized Pixel-Fitting (PPXF) routine (Cappellari & Emsellem 2004) and requires the use of a library of template spectra. We used 30 selected Evolutionary Population Synthesis (EPS) models presented by Bruzual & Charlot (2003), covering ages ranging from 5 Myr to 12 Gyr and three metallicities (0.004, 0.02, 0.05 Z$_\odot$). The emission-line profiles were fitted by Gaussian curves and we kept fixed the line ratios [O III]λ5007/[O III]λ4959 = 2.86 and [N II]λ6583/[N II]λ65484 = 2.94 to their theoretical values.

Due to the smaller spectral coverage and lower signal-to-noise ratio (S/N) of the GMOS data we were not able to use the same procedure to fit the GMOS spectra. Thus, we used the PROFIT code (Riffel 2010) to fit the emission-line profiles with Gaussian curves. The Gemini GMOS spectra of Akira include the following emission lines: H β, [O III] λλ4959,5007, [O I] λ6300, H α, [N II] λλ6548,83, and [S II] λλ6716,31, which are the most intense emission lines from the NLR of AGNs.

3 RESULTS

Fig. 1 shows maps of the H α flux measured from the MaNGA (left) and GMOS (right) data cubes. A similar behaviour is found for other emission lines. The emission-line flux distributions at large

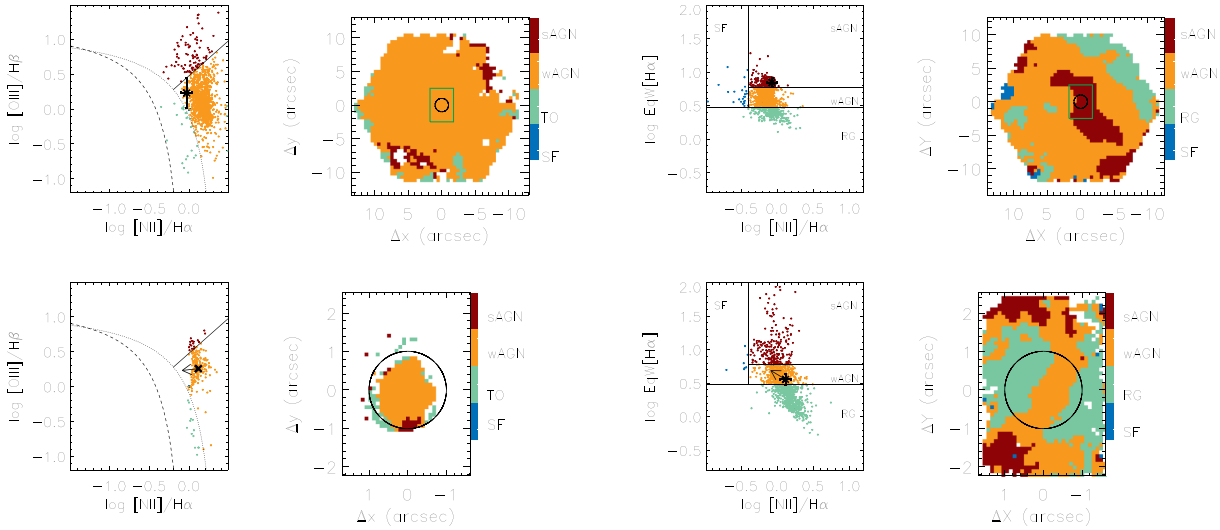

Figure 2. BPT (left, Baldwin, Phillips & Terlevich 1981) and WHAN (right, Cid Fernandes et al. 2010, 2011) diagrams from MaNGA (top) and GMOS (bottom) measurements. The colour coded excitation maps show the spatial location of each excitation region shown in the BPT and WHAN diagrams. The dashed line shown in the BPT diagram is from Kewley et al. (2001), the dotted line is from Kauffmann et al. (2003), and the continuous line is from Cid Fernandes et al. (2010). The following labels were used in the diagrams. SF: star-forming galaxies, TO: transition objects, wAGN: weak AGN (i.e. low-luminosity AGN), strong AGN (i.e. Seyferts) and RG: retired galaxies. The '×' symbol at the BPT and WHAN diagrams corresponds to the values obtained for the nucleus, as measured within an aperture of 2 arcsec diameter (identified in the excitation maps as black circles). For the GMOS diagrams, the arrows represent the measurements obtained after the subtraction of the stellar population component from the nuclear spectrum. The green rectangle overlaid to the MaNGA maps represents the GMOS FoV.

and small scales are distinct, with the orientation of the highest intensity levels misaligned by about 50°. Within the inner 1 arcsec (0.5 kpc) the GMOS flux map shows an elongation along PA≈−30°, while at distances larger than 5 arcsec from the nucleus, the most extended emission is seen along PA∼20°, as revealed by the MaNGA flux map. Based on the radio luminosity of Akira, Cheung et al. (2016) concluded that Akira harbours an LLAGN. Indeed, results from radio observations from VLA-FIRST data strongly suggest that most Red Geysers host an AGN (Roy et al. 2018). We have constructed the BPT (Baldwin et al. 1981) and WHAN (Cid Fernandes et al. 2011) diagrams (Fig. 2) in order to investigate the nature of the line emission in Akira. The WHAN diagram was originally introduced by Cid Fernandes et al. (2010) and first used for a large sample of galaxies observed as part of the SDSS by Cid Fernandes et al. (2011). This diagram is able to separate sources among (i) pure star-forming galaxies with log [N II]/H α < −0.4 and Equivalent Width (EW) for H α ($EW_{\rm H\,\alpha}$) >3 Å; (ii) strong AGN (sAGN; e.g. Seyfert nuclei) with log [N II]/H α > −0.4 and $EW_{\rm H\,\alpha}$ >6 Å; (iii) weak AGN (wAGN; e.g. LINERS) with log [N II]/H α > −0.4 and 3 Å<$EW_{\rm H\,\alpha}$ <6 Å; Retired Galaxies (RGs; i.e. fake AGN) with <$EW_{\rm H\,\alpha}$ <3 Å and passive galaxies (lineless galaxies) with EW < 0.5 Å for the H α and [N II]λ6583 emission lines.

Both GMOS and MaNGA BPT diagrams for Akira (Fig. 2) show that the emission-line ratios at most locations of the galaxy fall in the region occupied by LINERs and emission-line galaxies whose ionizing photons are produced in the atmospheres of evolved low-mass stars (Stasińska et al. 2008; Cid Fernandes et al. 2011; Singh et al. 2013; Belfiore et al. 2016). Since the BPT diagram is not efficient in discriminating between these two excitation agents, the WHAN diagram has been used; it shows that most of the gas emission in Akira is photoionized by an LLAGN. Integrating the fluxes within an aperture of 2 arcsec diameter centred at the nucleus, we find that in all diagrams the nucleus of Akira is classified as an AGN. It should be noticed that, as we are not subtracting the stellar population contribution spaxel-by-spaxel for the GMOS data cube, we may be underestimating the fluxes and Equivalent Width of the emission lines from the GMOS data, particularly important for the H lines. The arrows in the diagnostic diagrams show the location of the nucleus, if the stellar population is taken into account, as estimated by subtracting the stellar population contribution from the integrated spectrum. Thus, besides the radio emission, the observed line ratios also support the presence of an LLAGN in Akira.

The stellar and H α velocity fields and velocity dispersion (σ) maps of Akira are shown in Fig. 3. Considering the lower signal-to-noise ratio and spatial coverage of the GMOS data, we were able to measure the stellar kinematics only within the 1 arcsec central. We have masked out locations where the uncertainties in velocity or σ are larger than 25 km s^{-1}. These regions are shown in white in the stellar velocity field and in grey in the σ map derived from the GMOS data. We show all velocity fields and all σ maps at the same velocity scales, as labelled in the colour bars. The velocity fields are shown after the subtraction of the systemic velocity of the galaxy and the σ maps are corrected for the instrumental broadening. Although, no clear rotation pattern is observed for the stars in the inner region, the GMOS and MaNGA maps show similar range of values.

The stellar and gas kinematics of Akira measured from MaNGA data are distinct, as already noticed by Cheung et al. (2016). While the amplitude of the stellar velocity field about 50 km s^{-1}, the gas velocity field reaches projected velocities of up to 250 km s^{-1}. As already noticed by Cheung et al. (2016), the kinematic major axis (Ψ_0) of the stellar velocity field is distinct from that of the gas velocity fields. Using the kinemetry (Krajnović et al. 2006) method to symmetrize the MaNGA stellar velocity, we derived $\Psi_0 = 92°$ ± 11°, with blueshifts seen to the west and redshifts to the east. From the MaNGA H α velocity field, we obtain $\Psi_0 = 13°$ ± 5°, displaced by 79° from the stellar value. The orientation of the kinematic major axis is indicated as dashed lines in the MaNGA stellar and H α velocity fields, shown in Fig. 3. In addition, the

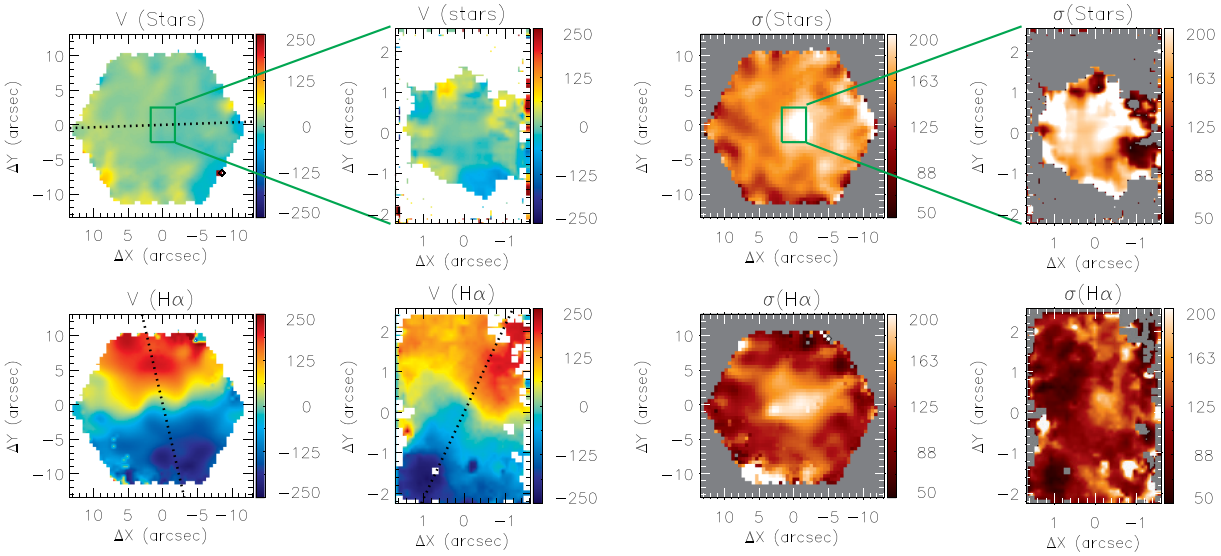

Figure 3. MaNGA and GMOS stellar and H α velocity fields (left-hand panels) and σ maps (right-hand panels). The dotted lines overlaid to the velocity fields show the orientation of the line of nodes (Ψ_0) as derived using the kinemetry method (Krajnović et al. 2006) for the whole field of view. From MaNGA data, we obtain $\Psi_0 = 92^\circ \pm 11^\circ$ for the stars and $\Psi_0 = 13^\circ \pm 5^\circ$ for the gas. For the GMOS H α velocity field, we obtain $\Psi_0 = 155^\circ \pm 3^\circ$ and were not able to constrain the Ψ_0 for the stars, due to the limited spatial coverage of the measurements. The colour bars show the velocity and velocity dispersion in units km s^{-1} after the subtraction of the systemic velocity of the galaxy and correct for the instrumental broadening, respectively.

GMOS H α velocity field shows that the orientation of the velocity gradient is distinct of that seen in the large-scale MaNGA map. Cheung et al. (2016) estimated the position angle of the major axis of Akira as ∼53°, based on the galaxy's elliptical isophotes (from the contours in their fig. 1c). This value is about 40° distinct than ours. However, it should be noticed that the isophotes of the galaxy are almost circular and thus the uncertainty in their determination of the orientation of the major axis of the galaxy may be very high.

The σ maps for the gas and stars show values ranging from 50 to 200 km s^{-1}, with the highest values observed at the nucleus of the galaxy. In the inner region, the σ values measured from MaNGA and GMOS data are consistent each other. For the gas, the GMOS map shows an 'S-shaped' structure of higher values which seems to follow the structure of highest H α emission seen in Fig. 1 and the higher ionization structure seen in the WHAN diagram of Fig. 2.

4 DISCUSSION

4.1 Gas kinematics

As already mentioned in previous section, we derive that the orientation of the line of nodes for the H α velocity field is $\Psi_0 = 13^\circ \pm 5^\circ$, as obtained using the kinemetry (Krajnović et al. 2006) method applied to the MaNGA data. We note that the velocity gradient in the inner region of Akira is distinct to that seen on large scales (see Fig. 4). Using the kinemetry method for the GMOS H α velocity field, we obtain that the main gradient is observed along $\Psi_0 = 155^\circ \pm 3^\circ$.

In order to verify if the observed velocity fields are consistent with motions dominated by the gravitational potential of the galaxy, we have derived the second velocity moment $V_{\rm rms} = \sqrt{V^2 + \sigma^2}$, where V is the line centroid velocity and σ its velocity dispersion. In Fig. 5, we present the plot of $V_{\rm rms}$ as a function of the distance from the nucleus. The $V_{\rm rms}$ was computed using the H α velocity and σ measurements within a pseudo-slit with width of 0.″5 and oriented along the main velocity gradients observed in the MaNGA (13°) and GMOS (155°) H α velocity fields. The dotted curves are from Cheung et al. (2016) and represent the predicted $V_{\rm rms}$ values by Jeans Anisotropic Modelling (JAM; Cappellari 2008) for two disc inclinations (i). The red curve corresponds to the predicted $V_{\rm rms}$ values for $i = 90^\circ$ and the blue line shows the predicted $V_{\rm rms}$ for $i = 46^\circ$, the minimum allowed axial ratio derived by the authors using GALFIT fits of the Hα flux distribution. More details about the dynamical modelling can be found in Cheung et al. (2016). As can be observed in Fig. 5 and already discussed by Cheung et al. (2016), the observed $V_{\rm rms}$ for MaNGA data exceed by up to ∼100 km s^{-1} the predicted values for disc rotation. In the inner region, a similar behaviour is observed for the GMOS data. For distances above 0.″5 from the nucleus, the observed values are more than 50 km s^{-1} higher than the dynamical model predictions.

Thus, considering that $V_{\rm rms}$ values derived from higher resolution GMOS data follow the same behaviour of the large-scale MaNGA data and exceed the predicted $V_{\rm rms}$ values by $\gtrsim 50$ km s^{-1}, we conclude that not only the large-scale gas kinematics, but also the kinematics in the inner few hundred parsecs cannot be described by disc-like rotation. Thus, as already concluded by Cheung et al. (2016), the most probably explanation for the observed gas kinematics of Akira is that it is due to centrally driven outflows.

4.2 The orientation of the outflow

In Fig. 4, we present the H α EW maps obtained from MaNGA (left-hand panel) and GMOS (right-hand panel) data. As for the flux maps shown in Fig. 1, the EW maps clearly show that the large- and small-scale structures are misaligned. The middle panels of Fig. 4 show the large (left) and small (right) scale H α velocity fields. Cheung et al. (2016) concluded that the large-scale gas kinematics observed for Akira cannot be explained by motions of the gas due to the gravitational potential of the galaxy, being most probably due to outflows from a central AGN.

In order to better investigate the gas kinematics and the origin of the suggested outflow in Akira, we have used the kinemetry method

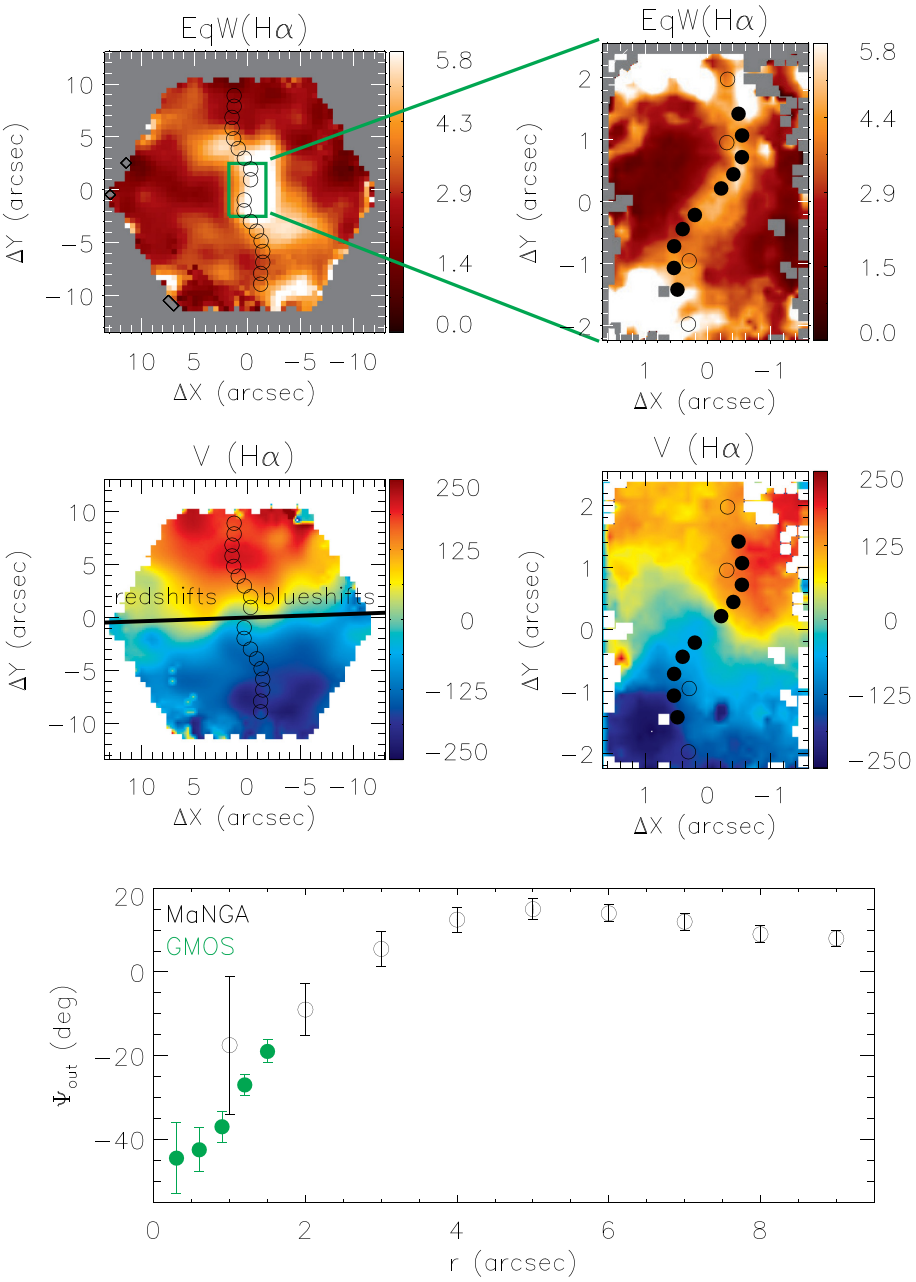

Figure 4. Large- and small-scale outflows in the *Akira* galaxy seen with SDSS-MaNGA and Gemini. Top: H α equivalent width (EW) maps from MaNGA (left) and Gemini (right) showing a stripe of larger values. *Middle:* large (left) and small (right) scale H α velocity fields. The black line shows the orientation of the line of nodes measured from the stellar velocity field, which is distinct of the orientation of the outflow. Regions where blueshifts and redshifts are seen is the stellar velocity field are labelled. The dots show the orientation of the outflow as derived using the kinemetry method. Filled circles are for Gemini GMOS data and open circles for MaNGA data. Bottom: variation of the orientation of the outflow with the distance from the nucleus.

to measure also the variation of orientation of the outflow (Ψ_{out}) with the distance from the nucleus using the H α velocity field, as it is the strongest emission line at most locations. For the GMOS data, we applied the kinemetry method for concentric rings of $r_w = 0\farcs6$ width by varying its distance to the nucleus in bins of $dr = 0\farcs3$. For the MaNGA data, we adopted $r_w = 2\farcs0$ and $dr = 1\farcs0$. These values were chosen based on the angular resolution of the data, so that in the inner disc the bin samples better the resolution of the data. In the bottom panel of Fig. 4, we present a plot of the orientation of the outflow Ψ_{out} versus the distance to the nucleus. We note that the orientation of the outflow changes from $\Psi_{out} \approx -50^\circ$ at the nucleus to $\Psi_{out} \approx 15^\circ$ at 5 arcsec from it. At larger distances, the value of Ψ_{out} shows a slight decrease.

4.3 The origin of the outflow

We have reported the detection of a varying orientation in the wind launched from the nucleus of Akira, as a function of distance from it. The intensity-line ratio diagnostic diagrams (Fig. 2) confirm that Akira hosts an AGN, therefore favouring the idea that the wind

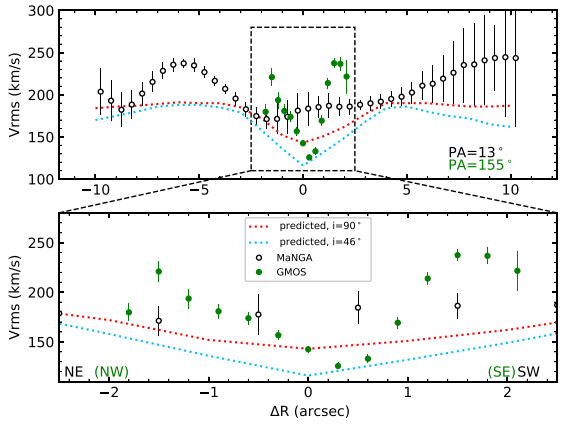

Figure 5. $V_{\rm rms}$ as obtained from MaNGA (open circles) and GMOS (closed circles) measurements, extracted along the orientation of the main velocity gradient seen in H α velocity field. The $V_{\rm rms}$ were calculated within a pseudo-slit with width of 0.″5 oriented along PA=10° for MaNGA data and 155° for GMOS data. The red and blue dotted curves show the predicted $V_{\rm rms}$ values by Cheung et al. (2016) for disc inclinations of 90° and 46°, respectively.

is launched by the SMBH rather than being supernovae-driven. In this section, we discuss the possible origins of the outflow and conjecture on the nature of the observed precession.

Akira shows point-like, core radio emission detected with VLA (Roy et al. 2018) and seems to be radio-loud, much like other LLAGNs (Ho 2002; Younes et al. 2012). Since it does not display evidence for the presence of any kpc-scale radio emission, Akira does not seem to produce extended relativistic jets like radio galaxies. For this reason, we think the outflow that we are tracing with MANGA and Gemini IFU optical observations is associated with a subrelativistic wind that spreads its power over a larger surface area than a collimated jet. In fact, such winds are expected to be a natural outcome of SMBHs accreting in the RIAF mode, as suggested by numerous theoretical works (e.g. Kurosawa & Proga 2008; Begelman 2012; Sadowski et al. 2013; Yuan et al. 2015; Bu et al. 2016).

Having established the likely wind-nature of the kpc-scale outflows observed in Akira, we now turn to the origin of the observed precession. First of all, most SMBHs should have some degree of angular momentum (Volonteri et al. 2005; King, Pringle & Hofmann 2008), even though it is not known how high the spin parameter is in the LLAGN population (Reynolds 2013). Secondly, there is no reason why the angular momentum vectors of the gas fed to the SMBH at large distances should know about the SMBH spin vector. Therefore, we should expect a natural misalignment between the accretion disc and BH spin leading to a torque exerted by the BH which introduces a global precession in the disc – the Lense–Thirring precession (Bardeen & Petterson 1975; Fragile et al. 2007). The precession should be manifested in any outflows originating from the disc due to angular momentum conservation (Liska et al. 2018, Liska, Fragile, private communication). We conclude that Lense–Thirring precession is a possible origin for the wind precession observed in Akira at kpc-scales. The change in the orientation in the ionized gas pattern (as seen in the EW maps of Fig. 4) also supports the precession of accretion disc.

We can use a simple argument to estimate the launching radius of the wind, assuming Lense–Thirring precession. From angular momentum conservation, we have

$$m\Omega r^2 = \text{constant} \tag{1}$$

throughout the wind, where m is the mass of a gas element, Ω is the wind precession angular velocity, and r is the distance to the SMBH. We apply the above equation to two separate regions of the flow – the footpoint in the accretion disc where the wind is launched and the location probed by the Gemini IFU observations at kpc-scales, from which it follows that

$$\Omega_d r_d^2 = \Omega_w r_w^2, \tag{2}$$

where the d and w subscripts refer to either the accretion disc or the wind. The above equation relates the measured wind properties at kpc-scales to the conditions closer to the black hole.

We can use equation (2) to estimate the distance from the SMBH at which the wind is launched, r_d. In order to do so, we need estimates of Ω_d, Ω_w, and r_w. From the lower panel of Fig. 4, we see that the wind completed a precession of about $\Delta\phi_w = 50°$. We can obtain an order-of-magnitude estimate of the time it takes to precess by this angle as the time it takes the wind to reach a distance of 5 arcsec from the SMBH (about 2.5 kpc). Using the current wind velocity as estimated by Cheung et al. (2016) of 310 km s^{-1}, the outflow will reach the above distance in $\Delta t_w < 10^7$ yr, assuming that the gas slowed down compared to its velocity at the launching point. We estimate, then,

$$\Omega_w = \frac{\Delta\phi_w}{\Delta t_w} \sim 10^{-7} \text{ rad yr}^{-1} \tag{3}$$

at $r_w = 2.5$ kpc. The calculation of the disc's Ω_w is model-dependent; from numerical, general relativistic magnetohydrodynamic simulations of tilted accretion discs, the disc precession frequency due to the Lense–Thirring effect is

$$\Omega_d \approx 2\pi \left(\frac{M}{10^8\,\mathrm{M}_\odot}\right)^{-1} \text{ rad yr}^{-1}, \tag{4}$$

where M is the SMBH mass (Fragile et al. 2007). Plugging in the above estimates of Ω_w, Ω_d, and r_w, equation (2) gives us a launching radius of

$$r_d \sim (0.1 - 1)\text{ pc} \sim \left(10^4 - 10^5\right) R_S, \tag{5}$$

where $R_S \equiv 2GM/c^2$ is the Schwarzschild radius, for a BH mass of 10^8 M$_\odot$ as appropriate for Akira. This launching radius is two to three orders of magnitude larger than expected from current theories of thermally driven or magnetically driven winds from RIAFs (∼10–100R_S; Sadowski et al. 2013; Yuan et al. 2015). This disagreement can be alleviated if the BH mass is much larger than 10^8 M$_\odot$ or if the disc precession frequency is considerably faster than current predictions of tilted, thick accretion disc models.

Another possible origin of precession of a wind could the Bardeen–Peterson precession (Bardeen & Petterson 1975; Caproni, Abraham & Mosquera Cuesta 2006) from a previous thin disc. This would be the case if Akira's nucleus was brighter in the past and its SMBH was correspondingly accreting at higher rates, and only more recently became underfed and turned into an LLAGN – similarly to Hanny's Voorwerp and IC 2497 (Lintott et al. 2009; Keel et al. 2012). This scenario is supported by the classical AGN feedback picture (Heckman & Best 2014), where the 'quasar mode' of accretion triggered by violent mergers halt the star formation, and when the quasar phase turns off, the 'maintenance mode' comes into effect from the underfed AGN and they become LLAGN.

Irrespective of the physical nature of the precession, when occurring on a wind it can increase its working surface, such that

the wind can spread its power over a larger area and stir up the ambient gas much more effectively than a narrow, collimated jet – i.e. precessing winds make AGN feedback more efficient for quenching star formation (e.g. Falceta-Gonçalves et al. 2010).

5 CONCLUSIONS

We used IFS obtained with the Gemini GMOS-IFU and SDSS-IV–MaNGA to investigate the gas kinematics of the galaxy Akira – the prototypical 'Red Geyser'. We found that the outflow can be resolved with GMOS-IFU down to the nucleus and changes orientation by about 50° from the nucleus of the galaxy to kiloparsec scales on a time-scale of 10^7 yr, being spatially correlated with the complex structure of high EW emission-line values. These observations are consistent with an origin in a precessing accretion disc. Precession in wide, subrelativistic outflows can help to spread their power over a larger area and increase the effectiveness of AGN feedback in galaxies similar to Akira. This could explain how a relatively low-power wind is none the less able to efficiently quench star formation and maintain the quiescence in typical galaxies.

ACKNOWLEDGEMENTS

We thank an anonymous referee for valuable suggestions which helped to improve the paper and acknowledge useful discussions with Chris Fragile, Matthew Liska, and Anderson Caproni. We thank an anonymous referee for valuable suggestions which helped to improve the paper. This study was financed in part by the Coordenação de Aperfeiçoamento de Pessoal de Nível Superior - Brasil (CAPES) - Finance Code 001, Conselho Nacional de Desenvolvimento Científico e Tecnológico (CNPq), and Fundação de Amparo à pesquisa do Estado do RS (FAPERGS). RN acknowledges funding by the Fundação de Amparo à Pesquisa do Estado de São Paulo (FAPESP) through grant 2017/01461-2.

Based on observations obtained at the Gemini Observatory, which is operated by the Association of Universities for Research in Astronomy, Inc., under a cooperative agreement with the NSF on behalf of the Gemini partnership: the National Science Foundation (United States), the Science and Technology Facilities Council (United Kingdom), the National Research Council (Canada), CONICYT (Chile), the Australian Research Council (Australia), Ministério da Ciência e Tecnologia (Brazil) and Ministerio de Ciencia, Tecnología e Innovación Productiva (Argentina).

SDSS is managed by the Astrophysical Research Consortium for the Participating Institutions of the SDSS Collaboration including the Brazilian Participation Group, the Carnegie Institution for Science, Carnegie Mellon University, the Chilean Participation Group, the French Participation Group, Harvard-Smithsonian Center for Astrophysics, Instituto de Astrofisica de Canarias, The Johns Hopkins University, Kavli Institute for the Physics and Mathematics of the Universe (IPMU) / University of Tokyo, the Korean Participation Group, Lawrence Berkeley National Laboratory, Leibniz Institut für Astrophysik Potsdam (AIP), Max-Planck-Institut für Astronomie (MPIA Heidelberg), Max-Planck-Institut für Astrophysik (MPA Garching), Max-Planck-Institut für Extraterrestrische Physik (MPE), National Astronomical Observatories of China, New Mexico State University, New York University, University of Notre Dame, Observatório Nacional / MCTI, The Ohio State University, Pennsylvania State University, Shanghai Astronomical Observatory, United Kingdom Participation Group, Universidad Nacional Autónoma de México, University of Arizona, University of Colorado Boulder, University of Oxford, University of Portsmouth, University of Utah, University of Virginia, University of Washington, University of Wisconsin, Vanderbilt University, and Yale University.

REFERENCES

Albareti F. D. et al., 2017, ApJS, 233, 285
Antonucci R., 1993, ARA&A, 31, 473
Baldwin J. A., Phillips M. M., Terlevich R., 1981, PASP, 93, 5
Barbosa F. K. B., Storchi-Bergmann T., McGregor P., Vale T. B., Rogemar Riffel A., 2014, MNRAS, 445, 2353
Bardeen J. M., Petterson J. A., 1975, ApJ, 195, 65
Begelman M. C., 2012, MNRAS, 420, 2912
Belfiore F. et al., 2016, MNRAS, 461, 3111
Benson A. J., Bower R. G., Frenk C. S., Lacey C. G., Baugh C. M., Cole S., 2003, ApJ, 599, 38
Blanton M. R. et al., 2017, AJ, 154, 28
Bower R. G., Benson A. J., Malbon R,, Helly J. C., Frenk C. S., Baugh C. M., Cole S., Lacey C.G., 2006, MNRAS, 370, 645
Bruzual G., Charlot S., 2003, MNRAS, 344, 1000
Bu D.-F., Yuan F., Gan Z.-M., Yang X.-H., 2016, ApJ, 823, 90
Bundy K. et al., 2015, ApJ, 798, 7
Cappellari M., 2008, MNRAS, 390, 71
Cappellari M., Emsellem, E., 2004, PASP, 116, 138
Caproni A., Abraham Z., Mosquera Cuesta H. J., 2006, ApJ, 638, 120
Cattaneo A. et al., 2009, Nature, 460, 213
Cheung E. et al., 2016, Nature, 533, 504
Cid Fernandes R., Stasińska G., Schlickmann M. S., Mateus A., Vale Asari N., Schoenell W., Sodré L., 2010, MNRAS, 403, 103
Cid Fernandes R., Stasińska G., Mateus A., Vale Asari N., 2011, MNRAS, 413, 1687
Cresci G. et al., 2015, A&A, 582, A63
Di Matteo T., Springel V., Hernquist L., 2005, Nature, 433, 604
Drory N. et al., 2015, AJ, 149, 77
Falceta-Gonçalves D., Caproni A., Abraham Z., Teixeira D. M., de Gouveia Dal Pino E. M., 2010, ApJ, 713, 74
Fischer T. C., Crenshaw D. M., Kraemer S. B., Schmitt H. R., 2013, ApJS, 209, 1
Fragile P. C., Blaes O. M., Anninos P., Salmonson J. D., 2007, ApJ, 664, 417
Gunn J. E. et al., 2006, AJ, 131, 2332
Harrison C. M., Costa T., Tadhunter C. N., Flutsch A., Kakkad D., Perna M., Vietri G., 2018, Nat. Astron., 2, 198
Heckman T. M., Best P. N., 2014, ARA&A, 52, 589
Ho L. C., 2002, ApJ, 564, 120
Hook I., Jorgensen I., Allington-Smith J. R., Davies R. L., Metcalfe N., Murowinski R. G., Crampton D., 2004, PASP, 116, 425
Hopkins P. F., Hernquist L., Cox T. J., Di Matteo T., Martini P., Robertson B., Springel V., 2005, ApJ, 630, 705
Ilha G.S. et al., 2018, MNRAS, 484, 252,
Karouzos M., Woo J.-H., Bae H.-J., 2016a, ApJ, 819, 148
Karouzos M., Woo J.-H., Bae H.-J., 2016b, ApJ, 833, 171
Kauffmann G. et al., 2003, MNRAS, 346, 1055
Keel W. C. et al., 2012, ApJ, 144, 66
Kewley L. J., Dopita M. A., Sutherland R. S., Heisler C. A., Trevena J., 2001, ApJ, 556, 121
King A. R., Pringle J. E., Hofmann J. A., 2008, MNRAS, 385, 1621
Krajnović D., Cappellari M., de Zeeuw P. T., Copin Y., 2006, MNRAS, 366, 787
Kurosawa, R., Proga, D., 2008, ApJ, 674, 97
Law D. R. et al., 2016, AJ, 152, 83
Lena D., 2014, preprint(arXiv:1409.8264)
Lena D. et al., 2015, ApJ, 806, 84
Lintott C. J. et al., 2009, MNRAS, 399, 129
Liska M., Hesp C., Tchekhovskoy A., Ingram A., van der Klis M., Markoff S., 2018, MNRAS, 474, 81
Oh K., Sarzi M., Schawinski K., Yi S. K., 2011, ApJS, 195, 130

Penny S.J. et al., 2018, MNRAS, 476, 979
Reynolds C. S., 2013, Class. Quantum Gravity, 30, 244004
Riffel R. A., 2010, Ap&SS, 327, 239
Riffel R. A., Storchi-Bergmann T., Riffel R., 2014, ApJ, 780, 24
Riffel R. A., Hekatelyne C., Freitas I. C., 2018, PASA, 35, 40
Roy N., 2018, ApJ, 869, 117
Sadowski A., Narayan R., Penna R., Zhu Y., 2013, MNRAS, 436, 3856
Sarzi M. et al., 2006, MNRAS, 366, 1151
Schmitt H. R., Donley J. L., Antonucci R. R. J., Hutchings J. B., Kinney A. L., 2003, ApJS, 148, 327
Schnorr-Müller A., Storchi-Bergmann T., Nagar N. M., Robinson A., Lena D., Riffel R. A., Couto G. S., 2014, MNRAS, 437, 1708
Singh R. et al., 2013, A&A, 558, 43
Smee S. A. et al., 2013, AJ, 146, 32
Smith J. et al., 2002, PASP, 114, 892
Springel V., Di Matteo T., Hernquist L., 2005, ApJ, 620, L79
Stasińska G. et al., 2008, MNRAS, 391, 29
Urry C. M., Padovani P., 1995, PASP, 107, 803
Venturi G. et al., 2018, A&A, 619, A74
Volonteri M., Madau P., Quataert E., Rees M. J., 2005, ApJ, 620, 69
Wake D. A. et al., 2017, AJ, 154, 86
Yan R. et al., 2016a, AJ, 151, 8
Yan R. et al., 2016b, AJ, 152, 197
Younes G., Porquet D., Sabra B., Reeves J. N., Grosso N., 2012, A&A, 539, A104
Yuan F., Gan Z., Narayan R., Sadowski A., Bu D., Bai X.-N., 2015, ApJ, 804, 101

This paper has been typeset from a TEX/LATEX file prepared by the author.